High Surface Area Tapes Produced with Functionalized Graphene

Sibel Korkut,[†,‡] Joseph D. Roy-Mayhew,[‡] Daniel M. Dabbs,[‡] David L. Milius,[‡] and Ilhan A. Aksay[‡,*]

[†]Vorbeck Materials Corporation, 8306 Patuxent Range Road, No. 105, Jessup, Maryland 20794, United States, and [‡]Department of Chemical and Biological Engineering, Princeton University, Princeton, New Jersey 08544, United States

ABSTRACT We describe a scalable method for producing continuous graphene networks by tape casting surfactant-stabilized aqueous suspensions of functionalized graphene sheets. Similar to all other highly connected graphene-containing networks, the degree of overlap between the sheets controls the tapes' electrical and mechanical properties. However, unlike other graphene-containing networks, the specific surface area of the cast tapes remains high (>400 $m^2 \cdot g^{-1}$). Exhibiting apparent densities between 0.15 and 0.51 $g \cdot cm^{-3}$, with electrical conductivities up to 24 $kS \cdot m^{-1}$ and tensile strengths over 10 MPa, these tapes exhibit the best combination of properties with respect to density heretofore observed for carbon-based papers, membranes, or films.

KEYWORDS: functionalized graphene · graphene paper · carbon tapes · tape casting · surface area

Networks of highly connected graphene offer significantly improved performance for a wide-range of devices including batteries,[1,2] sensors,[3] solar cells,[4,5] and supercapacitors.[6] But commercialization of these technologies requires large scale manufacturing of graphene networks using techniques that permit the simultaneous control of the surface area, degree of functionalization, electrical conductivity, and mechanical properties of the network. Current methods for fabricating interconnected graphene networks are limited to batch processes best suited for applications at the laboratory scale. Films of layered graphene networks are assembled layer-by-layer from monolayers formed in a Langmuir–Blodgett (LB) trough[7] or made by filtering graphene suspensions across a porous membrane.[8,9] The LB trough is impractical for fabricating films thicker than a few layers of graphene. Filtration produces dense and mechanically robust graphene networks, but the necessary filtration time is inversely proportional to the quality of the graphene suspension. Fabricating a graphene film of sufficient size for testing and evaluation or for use in a device can take over a week. We have circumvented the limitations of these small-scale processes using tape casting to produce polymer–graphene composite tapes from which the polymer is subsequently removed by thermolysis, resulting in large-area, highly connected graphene networks. The resulting tapes combine high surface area with superior electrical conductivity and mechanical strength when compared to other carbonaceous films, membranes, or papers.

Tape casting is the controlled casting of a colloidal suspension through a slit by the motion of a substrate relative to a doctor blade (Figure 1).[10] As it is a high throughput technique, tape casting requires large quantities of graphene, a need met by producing graphene *via* the simultaneous thermal exfoliation and reduction of graphite oxide.[11,12] This process yields large quantities of partially oxidized graphene sheets. In addition to oxygen-containing functionalities (epoxides, hydroxides, phenols, and carboxylic acids), the underlying graphene network contains lattice defects and vacancies (Figure 1, inset).[13] These functionalized graphene sheets (FGSs) can be distinguished by their oxygen content, which we relate to the carbon-to-oxygen ratio (C/O, mol/mol). The defects and oxygen-containing groups cause the sheets to wrinkle, reducing the area of contact between sheets and preventing stacking, an advantage for high surface area applications.[1,2,6] Further, the defect sites and the functional groups on FGSs have been shown to increase the chemical activity of the sheets, which is favorable for electrochemical sensors,[3,14] catalysts,[15] and fuel cells.[16]

For this work, we used tape casting to fabricate long (>1 m) and wide (up to 15 cm to date) FGS/polymer composite tapes which could then be cut to any shape. Self-supporting, electrically conducting, large-area FGS tapes were produced by removing the polymer matrix and the surfactant from the composite tapes. These tapes can be used in a variety of applications such as electrodes in supercapacitors and sensors, or as scaffolds for the active

* Address correspondence to iaksay@princeton.edu.

Received for review April 13, 2011 and accepted May 5, 2011.

Published online 10.1021/nn2013723

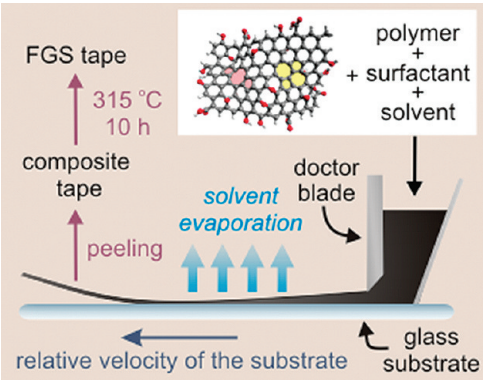

Figure 1. Schematic describing the production of FGS tapes. The FGS schematic shows a sheet's defective and wrinkled structure. Oxygen functionalities are shown in red, a 5−8−5 defect is pink and a 5−7−7−5 defect is yellow.

material in Li-ion batteries and dye-sensitized solar cells.[1−4,6] In the following sections, we first describe how FGS tapes were produced and discuss their general structure. We then analyze their electrical and mechanical properties by focusing on the structural changes caused by different heat treatments. Finally, we compare the properties of FGS tapes to those of other carbonaceous materials and discuss the structural features of the FGS tapes that underlay their superior properties.

RESULTS AND DISCUSSION

Preparation of FGS Tapes. Fabrication of high surface area tapes begins by preparing highly dispersed suspensions of FGSs. To disperse FGSs in water we used a triblock copolymer surfactant (ethylene oxide$_{100}$-propylene oxide$_{65}$-ethylene oxide$_{100}$, *i.e.*, $EO_{100}PO_{65}EO_{100}$). This surfactant is compatible with the binder polymer (poly(ethylene oxide), *i.e.*, PEO) and does not leave any metallic residues upon carbonization. The amount of surfactant needed to disperse the sheets was determined by measuring the FGS concentrations in the supernatant of suspensions containing different amounts of surfactants and comparing that to the initial overall suspension concentration (Figure 2a). The amount of FGS in the supernatant was observed to increase with increasing surfactant concentration, indicating improved suspension stability, until the FGS concentration plateaued at the initial concentration near a surfactant-to-FGS ratio of 1 (g/g) (Figure 2a). This behavior is typical for a sterically stabilized suspension,[17] where increased surface coverage of the particles increases the suspension stability.[18] $EO_{100}PO_{65}EO_{100}$ adsorbs on carbon surfaces through its hydrophobic PO chain and extends its hydrophilic EO chains into water.[19] Since water is a good solvent for EO, the interaction between EO chains provides a repulsive barrier preventing the aggregation of FGSs.

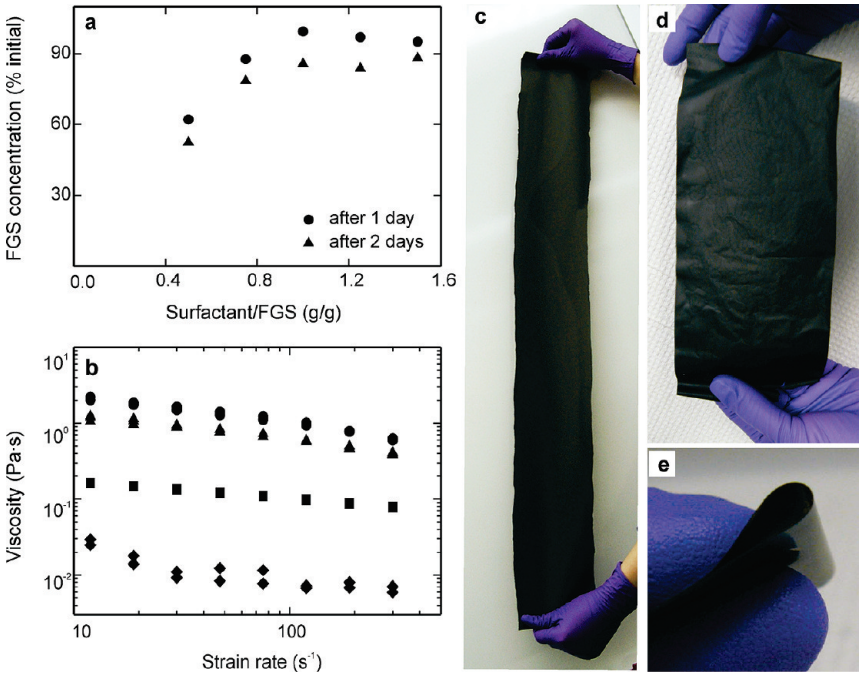

Figure 2. (a) Supernatant concentration given as percentages of initial concentration (0.5 mg·mL^{-1}) as a function of surfactant to FGS ratio, 1 day and 2 days after the preparation of suspensions by tip sonication. The linear relationship between the height of the absorbance peak at 280 nm and the FGS concentration is used for determining the concentrations of aqueous FGS-surfactant suspensions. (b) Viscosity as a function of strain rate for the suspension used for casting of the (●) 15 wt % FGS containing composite tape (2.8 wt % PEO, 0.6 wt % FGS, 0.6 wt % surfactant in the suspension), (▲) PEO solution (2.8 wt % PEO), (■) tape casting suspension used for casting of the 40 wt % FGS containing composite tape (0.68 wt % PEO, 1.36 wt % FGS, 1.36 wt % surfactant in the suspension), and (♦) FGS suspension (0.6 wt % FGS, 0.6 wt % surfactant). (c) A self-supporting FGS/polymer/surfactant composite tape after being removed from the tape casting substrate. (d and e) FGS tapes after thermolysis of polymer and surfactant.

If the coverage of FGS by surfactants is not complete, the FGSs can aggregate due to van der Waals forces. Therefore, a plateau in the dispersion concentration implies saturation of FGS surfaces by surfactant molecules. The decrease in supernatant concentrations over time (Figure 2a) indicates sedimentation of FGSs from aged suspensions. This result suggests aggregation of FGSs. Although this process is not fully understood, it could take place through van der Waals interactions upon desorption of weakly adsorbed surfactant.[20,21] However, as both tape casting and drying were complete within two days, the adsorption of the triblock copolymer on FGSs was found to be adequate for effective tape casting.

In addition to maintaining a sufficient degree of dispersion for the duration of the casting process, tape casting suspensions need to flow easily through the gap between the blade and substrate under shear (Figure 1), and maintain the shape and thickness of the cast tape once shearing is removed after exiting the blade. This type of behavior is typically achieved by tape casting shear thinning suspensions; however, as discussed below, the wettability of the substrate and pinning of the contact line may also play an important role. The tape casting suspensions used for this study exhibited shear thinning behavior under the shear rates used in their casting, $\sim$100 s^{-1} (Figure 2b). This was a result of shear thinning behavior of both the PEO solutions and the FGS suspensions (Figure 2b) due to the disentanglement of PEO molecules, the break-up of the FGS network, and the orientation of both FGSs and PEO molecules under shear.[22,23] The viscosities of the FGS tape casting suspensions varied within 1 order of magnitude at a fixed strain rate, with suspensions having the highest FGS and thus lower PEO content exhibiting the lowest viscosity. The viscosity of the suspension increased with increasing PEO content; the PEO solution with comparatively higher viscosity (Figure 2b) acted as a thickening agent and was used to tune the suspension viscosity. When the shear rate was decreased from 100 to 1 s^{-1} the viscosity of the cast suspension took 1–2 s to return to the viscosity exhibited under a shear rate of 1 s^{-1} (Supporting Information Figure S1). Therefore, the viscosity of the suspensions rose substantially within a few seconds of being cast. However, when cast on nonwetting substrates on which the contact line was not sufficiently pinned,[24] the suspension pulled away from the substrate and cohered into a formless puddle, demonstrating that the zero shear viscosity of the suspensions was not high enough to maintain the shape of the cast tape. Casting the suspension on a wetting substrate (see Methods section) on which the contact line was pinned overcame this difficulty maintaining the tape's shape during solvent evaporation.

The cast and dried tapes were easily removed from the substrate, producing free-standing, continuous composite tapes up to 15 cm wide (Figure 2c). The size of these tapes was limited only by the width of the doctor blade and the width and length of the substrate; hence, even larger composite tapes are feasible using this approach. Subsequent heating of the composite tapes at 315 °C removed most of the polymer and surfactant (Supporting Information Table S1), and the resulting FGS tape remained flexible and mechanically robust (Figure 2d,e).

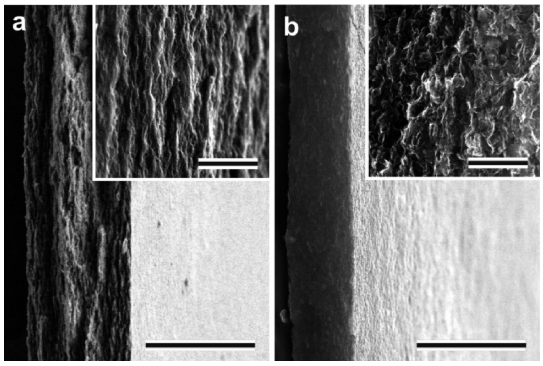

Figure 3. Microstructure of FGS tapes. SEM images of FGS tapes with (a) 0.40 and (b) 0.15 g·cm^{-3} density. Insets show increased magnification of the tape cross section. The scale bars show 50 μm for the main images and 5 μm for the insets.

Structural Features. FGS tapes exhibited uniform thickness and a defect-free microstructure (Figure 3). The absence of microscale cracks within the FGS tapes suggests that thermolysis was done slowly enough to allow the evolved gases to escape from the tape without creating structural defects. Furthermore, the linear dependence of density on initial FGS concentration (Supporting Information Figure S2) implies that the volume occupied by the polymer and surfactant was simply replaced by air-filled pores during thermolysis.

The structure of the tapes changed with the FGS concentration in the initial composite tape. An anisotropic structure was observed in the cross-section of the denser tapes (*i.e.*, higher FGS concentration in the composite tape), with striations parallel to the tape surfaces running along the long axis of the tape (Figure 3a). At lower densities this structure was lost and the cross-section of the low density tape appeared more isotropic (Figure 3b). The anisotropy is most likely caused by the alignment of the graphene sheets, which could take place due to the constrained rotational motion of FGSs with increasing FGS content.[25] Alignment of FGS due to shear during the tape casting process is also expected since the rotary Peclet number is large (Pe $\approx 10^4$–10^5 even when the rotary diffusivity is calculated based on dilute conditions).[26] However, as there was sufficient time during solvent evaporation for rotational Brownian motion to randomize the orientation of FGSs after shearing, the anisotropic structure of the tapes is most likely not due to shear during the casting process.

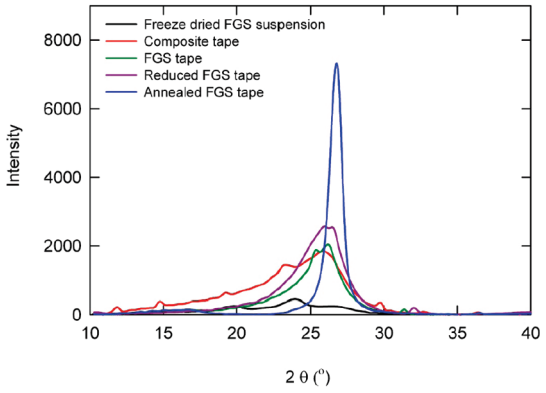

Figure 4. XRD spectra of composite and heat-treated tapes and a freeze-dried sample of an FGS/surfactant suspension used for the preparation of a tape casting suspension. PEO diffraction peaks (~20° and ~24°) are apparent only in the spectra of the freeze-dried suspension and composite tape.

The degree of graphene restacking in our FGS tapes was monitored through X-ray diffraction (XRD) analysis (Figure 4), the presence of graphite being indicated by the appearance of a diffraction peak centered at an angle of 26.4°. The amount of scattering was very low for powders formed by freeze-drying suspensions of FGS. The graphitic peak was seen to be higher for the composite tape, implying that FGSs partially reassembled into stacked structures during solvent evaporation. Further, the little difference that was seen to exist between the diffraction intensities of the composite and thermolyzed FGS tapes showed that removing most of the polymer and surfactant from the composite tape (Supporting Information Table S1) had little effect on the degree of graphitization (Figure 4).

A degree of graphene restacking is required to fabricate self-supporting, three-dimensional graphene networks, but stacks of FGSs containing more than a few sheets must be avoided to more fully exploit graphene's properties.[27] Therefore, the amounts of graphitic and graphene regions need to be balanced to combine a mechanically robust tape with more graphene-like properties, such as high surface area and electrical conductivity. Even though some graphitization occurred during their preparation, the surface area of FGS tapes was significantly higher than the values reported for graphene networks formed by evaporative drying of suspensions of flatter graphene sheets (44 $m^2 \cdot g^{-1}$).[28] Our conjecture is that the crumpled structure of FGSs[11,12] limits the contact area between adjacent sheets, whereas flattening the sheets increases the degree of overlap and results in a lower surface area.

FGSs can be flattened and the spacing between the sheets reduced through thermal treatment (Supporting Information, Figure S3). XRD patterns from FGS tapes heated to 1000 °C ("reduced FGS tapes") did not appear to be significantly affected by the higher temperature treatment (Figure 4), indicating that the FGSs were not significantly flatter than those in the FGS tapes. Although the oxygen content of the sheets was lowered, the apparent density and surface area of the tapes were only slightly different from those of the FGS tapes treated at 315 °C (Supporting Information Figure S2 and Figure S4). However, heating the tapes to 2250 °C ("annealed FGS tapes") had a significant effect on the intensity of the XRD peaks (Figure 4). The higher temperature of annealing partially restored the sp^2 network within the sheets[29] causing the sheets to flatten (Supporting Information Figure S3). The flatter sheets then stacked more readily (Figure 4), increasing the apparent density by 17 to 49% when compared to FGS tapes and decreasing the surface area to ~200 $m^2 \cdot g^{-1}$ (Supporting Information Figure S2 and Figure S4).

Electrical Properties. The electrical conductivity of the FGS tapes changed by 2 orders of magnitude, from 130 to 24000 $S \cdot m^{-1}$ depending on the FGS concentration and the heat treatment protocol (Figure 5a). Increasing the FGS concentration in the tapes increased the number of conductive paths in the sample and resulted in higher conductivities. We separated the effect of heat treatment on FGSs from that on the polymer and surfactant by comparing the electrical properties of the tapes with those of pellets formed by compressing FGS without any binders ("FGS pellets"). At a given FGS concentration, the conductivity of the tapes doubled following the removal of the polymer and the surfactant at 315 °C and increased another order of magnitude when reduced at 1000 °C (Figure 5a). The pellets' conductivity also increased when heated at 315 °C, but to a smaller extent. These observations suggest that a significant part of the increase in the FGS tape's conductivity during the first heat treatment was due to decreasing the contact resistance between the FGSs simply by removing the polymer and surfactant. A smaller effect resulted from changes in the FGSs themselves, seen as an increase in C/O from 13 to 17.[30] A further 8 to 10-fold increase in conductivity was exhibited by both the reduced (1000 °C) tapes and reduced pellets. Since the pellets did not contain any material other than FGS, we conclude that the conductivity of the tapes was strongly affected by the changes in FGS, particularly the drastic increase in C/O, but not so much by changes in the polymer and surfactant residues upon reduction (Supporting Information Table S1).

Extrapolating the measured relationships between conductivity and the density for reduced and annealed FGS tapes (Figure 5a) to the density of graphite (1.84 $g \cdot cm^{-3}$)[31] gives values of 1.0×10^5 $S \cdot m^{-1}$ and 1.2×10^5 $S \cdot m^{-1}$, respectively. These are very close to the conductivity of polycrystalline graphite (1×10^5 $S \cdot m^{-1}$)[32] but lower than the conductivity of highly ordered pyrolytic graphite (HOPG) or single graphene sheets (Figure 3a), indicating that the contact

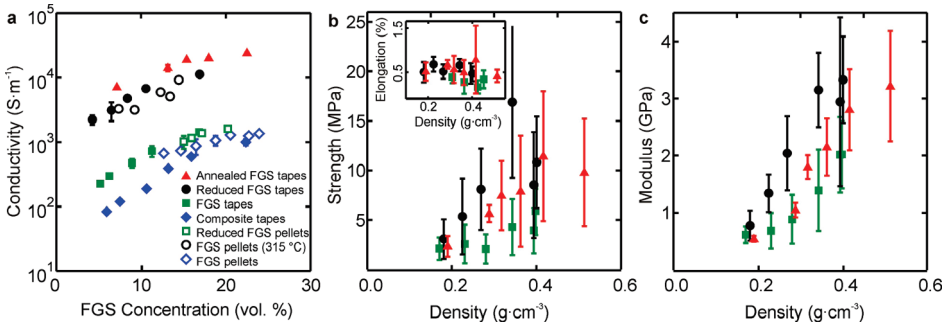

Figure 5. The effect of heat treatments on tape properties. (a) Conductivity as a function of FGS concentration in the tapes and compressed FGS pellets; (b) tensile strength; (c) modulus and elongation at break (inset of panel b) of the tapes as a function of apparent density. Standard deviations are calculated for each point from three or more identically prepared samples.

resistance between the sheets played a significant role in the conductivity of the tapes. Annealing at 2250 °C resulted in a 50 to 300% increase in conductivity over that of the reduced FGS tapes, and the conductivity reached a maximum measured value of 24 kS·m^{-1} (Figure 5a). This improved tape conductivity may have resulted from increasing FGS conductivity due to removing defects and increasing C/O (from 247 to 371),[30] as well as decreasing contact resistance. Both the decrease in separation between sheets, caused by the removal of oxygen-containing functional groups and the increase in contact area, due to flatter sheets, contributed to a lower contact resistance.

Mechanical Properties. Both the strength and the modulus of FGS tapes increased with increasing density, a measure of the increasing volume fraction of FGSs in the tapes (Figures 5b,c). Within a unit cross-sectional area, higher volume fractions of FGSs increased the load-carrying area, raising the strength of the tape. The increase in modulus with density is well-known for porous materials.[33] The modulus, E, of a porous network whose skeleton is held together by covalent or ionic bonds exhibits a power-law dependence on the density ρ, $E \sim \rho^n$; where the exponent n falls between the limits of 2 and 3 depending on the pore structure.[33,34] Interestingly, n is between 1.5 and 1.9 for our tapes. The most likely reason for low n is that the FGS network is held together by weak van der Waals forces.[35] The increase of n from 1.5 to 1.7 upon reducing FGS at 1000 °C and to 1.9 upon annealing FGS tapes at 2250 °C supports this hypothesis. While the bonds between the graphene sheets remained weak, the spacing between FGSs decreased concomitantly with increasing contact area during heating, both of which increased the extent of van der Waals bonding within the network.

Extrapolating the respective relationships between the tapes' strength and modulus to density (Figure 5b,c) we observe that the strength and modulus of the tapes (25−142 MPa, and 20−55 GPa) are similar to those of polycrystalline graphite (30 MPa and 18 GPa, respectively),[31] when extrapolated to the density of graphite (1.84 g·cm^{-3}).[31] These values are orders of magnitude lower than the strength and modulus of a single sheet of graphene (130 GPa and 1.0 TPa, respectively)[36] indicating that the mechanical properties of the tapes were not governed by the in-plane properties of the graphene sheets. Instead, the tapes' mechanical properties were determined by the weak interactions (*i.e.*, van der Waals forces and frictional forces) between the sheets. The wrinkled topography of reduced FGSs is expected to hamper sliding of the sheets over one another, enhancing the frictional forces and resulting in a higher strength and modulus. Annealed FGS tapes are flatter (Supporting Information Figure S3), containing less oxygen and fewer defects, and the spacing between the annealed sheets is smaller. These countervailing properties led to strengths and moduli observed to lie between those of FGS and reduced FGS tapes (Figure 5b,c). As in other layered materials, a significant elongation in comparison to brittle materials, ∼ 0.5% (inset of Figure 5c), is observed and can be explained as the distributed deformation due to the sliding of overlapping regions through a strain hardening mechanism. Even without binder, the strength of current FGS tapes meets or exceeds the strength range (0.55−5.5 MPa) of green tapes (here, green tapes refer to composite tapes of ceramic particles and binder commonly used to manufacture microcircuits) used in commercial electronic applications, suggesting that FGS tapes are strong enough to be handled and processed in a similar, industrial-scale, manner.[37−39]

Comparison of FGS Tapes with Other Carbonaceous Materials. The FGS tapes had lower density compared to those of other carbonaceous networks, while exhibiting high surface area, good electrical conductivity, and robust mechanical properties (Figure 6a−d). We attribute this combination of features to the consolidation of FGSs during tape casting and thermolysis that resulted in a "patch-quilt" structure. In this model, crumpled graphene sheets are randomly interwoven and stitched together by overlapping, graphitic junctions. The resulting graphene−graphite hybrid contains regions of single wrinkled sheets, enhancing the overall surface area, plus graphitic regions composed of partially

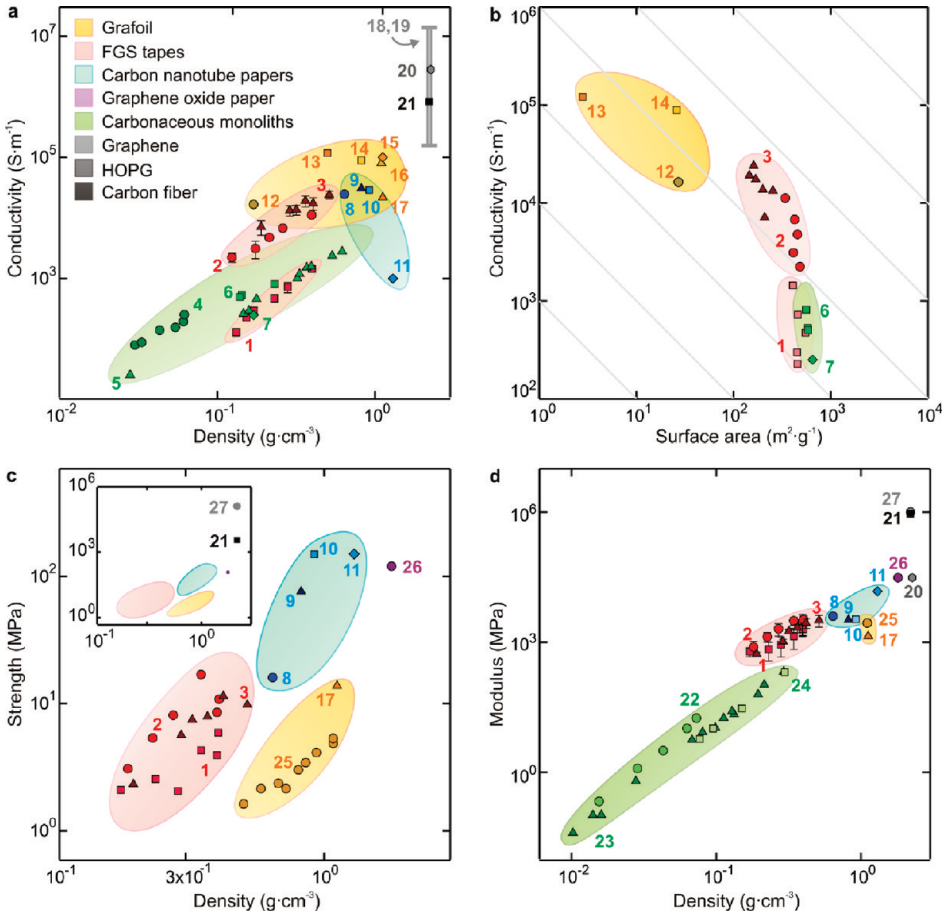

Figure 6. Comparison of carbonaceous materials. Panels a−d compare electrical and mechanical properties and surface area of our tapes with the corresponding properties of other carbonaceous films, tapes, and monoliths. The diagonal lines in panel b represent constant values for the multiplication of conductivity with surface area and are plotted to guide the eye. Both high conductivity and high surface area are desirable for electronic applications. Although the relative importance of each attribute is device specific, we assume an equal weighting to conductivity and surface area, thus the higher the diagonal, the better device performance. Standard deviations are calculated from three or more identically prepared samples. (1) FGS tapes, (2) reduced FGS tapes, (3) annealed FGS tapes, (4) carbon monoliths containing 30 wt % carbon nanotubes,[42] (5) carbon monoliths without carbon nanotubes,[42] (6) carbon monoliths with 8 wt % double-walled carbon nanotubes,[43] (7) carbon monoliths,[43] (8) carbon nanotube paper using Triton-X as dispersant,[40] (9) carbon nanotube paper using DNA as dispersant,[40] (10) carbon nanotube paper using chitosan as dispersant,[40] (11) carbon nanotube ribbons,[41] (12) Grafoil foam,[48,49] (13) ZYX (Grafoil-like material produced from HOPG),[48−50] (14) Grafoil,[48] (15) ZYX,[50] (16) Grafoil,[50] (17) Grafoil,[51] (18) graphene intrinsic conductivity (calculated from carrier density of 10^{12} cm^{-2} and mobility of 200,000 $cm^2 \cdot V^{-1} \cdot s^{-1}$),[52] (19) graphene intrinsic conductivity (no charge carriers),[53] (20) HOPG[54,55] (21) carbon fibers,[44] (22) carbon monoliths containing >16 wt % carbon nanotubes,[43] (23) carbon monoliths containing <16 wt % carbon nanotubes,[43] (24) carbon monoliths from carbonized resorcinol,[34] (25) Grafoil,[56] (26) graphene oxide paper,[9] (27) pristine graphene.[36]

overlapping sheets, which increase the strength and modulus. This structure allows for high surface area to be maintained, and the FGS tapes exhibited values an order of magnitude higher than those measured for Grafoil tapes with equivalent densities (Figure 6a,b). The strength of FGS tapes matched or exceeded the strength of Grafoil despite having only half of the apparent density (Figure 6c). At the time of writing, the FGS tapes exhibited the highest conductivities among self-supporting carbonaceous papers and monoliths such as those composed of Grafoil, carbon nanotubes,[40,41] or carbonized polymers (Figure 6a).[42,43] (Higher conductivity for Grafoil has been reported in one publication but, by the time of writing, this has been the only document reporting such high values. Furthermore, the method to determine the reported conductivities has been called into question[48] as it involved compressing the sample during testing, thereby increasing the density.) Finally, the modulus of our tapes was determined to be higher than the moduli reported for other carbonaceous materials, when compared at equivalent densities (Figure 6d), and had comparable or higher strengths (Figure 6c).

To our knowledge, the only macroscopic carbonaceous materials which surpass the strength and modulus of our tapes per density at the time of writing are carbon fibers.[44] The high strength and modulus of carbon fibers (exceeding 6 GPa strength and 800 GPa modulus) are explained by orienting graphitic zones along the fiber's longitudinal axis and the extent of

cross-linking between these zones,[45] which, unlike the carbonaceous tapes and papers, allow the load to be carried by the strong carbon−carbon bonds. This comparison suggests that improving the mechanical properties of our FGS tapes while maintaining the surface area and electrical conductivity could be achieved by cross-linking the sheets using covalently bound bridges.

CONCLUSIONS

Tape casting of FGS-polymer composites followed by thermolysis of the polymer provides an industrially scalable way of producing large, free-standing and high surface area FGS tapes having a patch-quilt structure. We have shown that the density (0.15−0.51 $g \cdot cm^{-3}$), BET surface area (200−500 $m^2 \cdot g^{-1}$), electrical conductivity (130−24000 $S \cdot m^{-1}$), strength (2−17 MPa) and modulus (0.6−3.3 GPa) of FGS tapes can be tuned by adjusting the FGS concentration in the composite tapes and the heat treatment protocols. Increasing the FGS concentration increased all aforementioned properties except the surface area, which remained constant. Reduction at 1000 °C improved the conductivity, strength, and modulus; however, it did not affect the density or the surface area determined using nitrogen adsorption. Annealing at 2250 °C enhanced the graphitization, which reduced the surface area and densified the material. Consequently, annealing further increased the conductivity at the expense of the strength and the modulus. Comparison with the current literature shows that the values of conductivity, strength, and modulus of these tapes, per density, meet or exceed those of all other high surface area carbonaceous tapes or paper-like materials.

METHODS

Preparation of FGS Tapes. The fabrication of FGS tapes began with the production of FGS/surfactant/organic binder composite tapes, which were cast from a suspension of FGS stabilized with a poly(ethylene oxide)−poly(propylene oxide)−poly(ethylene oxide) ($EO_{100}PO_{65}EO_{100}$) triblock copolymer surfactant (F-127, Pluronic, Sigma-Aldrich, St. Louis, MO) in an aqueous poly(ethylene oxide) (PEO, M_v = 600 000; Sigma-Aldrich) binder solution. To produce the FGS (Vor-x, Vorbeck Materials Inc., Jessup, MD) suspensions, we first prepared an $EO_{100}PO_{65}EO_{100}$ surfactant solution with an equal amount of surfactant (by mass) to that of the FGSs to be added in deionized water (typically >16 MΩ). The equal mass of surfactant to FGS corresponded to adequate coverage of FGS by surfactant to ensure a stable dispersion for the duration of the tape casting process. Then, over a period of 1 h, the FGS suspension was slowly added to the surfactant solution under continuous stirring and ultrasonication at 30% power (Vibra Cell, Sonics & Materials Inc., Newtown, CT) while kept in an ice bath to prevent heating. The suspension was then centrifuged at 900*g* for 10 min to remove any remaining agglomerates, and the supernatant was decanted. The FGS concentration of this supernatant, measured using UV−vis spectroscopy (model 9430, IBM, Armonk, NY), was typically ∼1.6 wt %. These refined suspensions were then transferred to a vacuum chamber and stirred under slight vacuum to remove entrained air.

Binder solutions of 4.5 wt % PEO were prepared by first adding the PEO powder to absolute ethanol (Acros, Geel 2440, Belgium) under continuous stirring at 65 °C and then adding an equal volume of water. Premixing the PEO with ethanol prevents the formation of clumps and facilitates the homogeneous dispersion of the PEO. Stock PEO solutions were then added to the FGS/surfactant suspensions to obtain FGS/surfactant/PEO tape casting suspensions having the desired weight ratios. The tape casting suspensions were stirred for at least 2 h prior to casting.

Rheological measurements (Rheometrics Fluid Spectrometer RFS-II, Rheometrics Inc., Piscataway, NJ) were done using a parallel plate fixture (diameter: 5 cm). The temperature of the fixture and the sample was kept constant at 25 °C using a temperature controlled water bath (Rheometrics Environmental Control Circulator, Rheometrics, Inc.).

The glass plates on which the tapes were cast were prepared by first cleaning their surfaces using detergent followed by 1 M KOH (aq) solution (Acros). After rinsing and drying, the surfaces were treated with a mixed silane solution [a mixture of 6.6 mM octadecyltrichlorosilane (Sigma-Aldrich) and 3.3 mM aminopropyltriethoxy silane (Sigma-Aldrich) in hexane (Acros)] then dried to reduce the adhesion between the glass and the composite tape. Without this silane treatment, the tapes could not be peeled cleanly off the glass.

The FGS/surfactant/PEO suspensions were cast on the silane-coated glass plate using a doctor blade assembly (model SDBA, Richard E. Mistler, Inc., Morrisville, PA) with a 1.5 mm blade gap in a class 1000 soft wall clean room (model DFE1214-7, Atmos-Tech Industries, Ocean, NJ). The tapes were dried in the clean room at ambient temperature for several days and then removed from the glass templates to obtain large, free-standing tapes.

The thermolysis of the binder and surfactant from these composite tapes was done in a graphite-element furnace (model 1000, Thermal Technology LLC, Santa Rosa, CA). To heat many samples in each batch, composite tapes were stacked alternating with Grafoil sheets (GTB grade, 125 μm thick, Union Carbide, Cleveland, OH). The pressure in the furnace chamber was first reduced to 100 mTorr and then backfilled with dry nitrogen to atmospheric pressure in order to decompose the organics in a nonoxidizing atmosphere. Thermolysis runs were done under flowing nitrogen at 2 SCFM (3.4 $m^3 \cdot h^{-1}$). The furnace chamber was heated to 90 at 5 $°C \cdot min^{-1}$, held for 1 h to remove volatiles, then heated to 315 at 5 $°C \cdot min^{-1}$ and held at the higher temperature for 10 h. When higher temperatures were used for subsequent processing, the furnace temperature was raised at 10 $°C \cdot min^{-1}$ to the target temperature. As dissociation of nitrogen becomes appreciable above 1237 °C, for heat treatments above 1000 °C, argon was used in the furnace chamber as the inert atmosphere.

Preparation of FGS Pellets. FGS pellets, comprising only compacted FGSs, were used to distinguish between the contributions of FGSs and the thermolyzed surfactant and PEO to the conductivity of FGS tapes and reduced FGS tapes. By compressing *ca.* 100−150 mg of FGSs using a cylindrical stainless steel die with inner diameter of 2.9 cm and height of 4.4 cm under a hydraulic press (Carver Laboratory Press, model-C, Fred. S. Carver Inc., Menemonee Falls, WI) brittle FGS pellets were formed. The density of the pellets was adjusted by varying the load between 40 and 150 MPa. Subsequent heat treatments for the pellets were done under the same conditions used for the thermolysis of the composite tapes and reduction of FGS tapes.

Preparation of Freeze Dried FGS Powder. To probe the effect of solvent evaporation on the graphitization of FGSs, freeze-dried samples were prepared. To freeze-dry an FGS suspension that has been sonicated, deaired, and classified as previously

described, the suspension was added dropwise to the ultrasonicator probe at 60% power (Vibra Cell). When the drop reached the tip of the probe it vaporized and settled into a bath of liquid nitrogen stirred by a propeller creating a frozen suspension. This frozen suspension was then placed in an insulating container and freeze-dried (Virtis AdVantage, Gardiner, NY) at 50 mTorr for 96 h.

Characterization. The density of the tapes was determined by measuring the dimensions and weight of rectangular pieces. The densities for three samples were measured for each FGS concentration and the average density was reported. The volume fraction of the FGSs in the tapes was determined assuming a FGS density of 2.2 $g \cdot cm^{-3}$, the density of graphite as calculated from the hexagonal carbon lattice with an interlayer graphitic spacing of 0.34 nm.

Composite tapes were examined by simultaneous thermal analysis (STA; 449 C Jupiter, Erich Netzsch GmbH & Co., Germany) incorporating a thermogravimetric analyzer (TGA) and a differential scanning calorimeter (DSC). Aluminum pans were used and all STA measurements were done under flowing dry nitrogen (40 $mL \cdot min^{-1}$). The DSC was calibrated using a set of standards (In, Sn, Bi, Zn, CsCl) with well-known temperatures and enthalpies of phase transitions. TGA runs of composite tapes were performed to determine the onset of decomposition and the required duration of the heat treatment. Two runs of thermal analysis were done: in the first run the temperature was increased at a rate of 1 $°C \cdot min^{-1}$ and the decomposition temperature was determined; in the second run, the sample was held at the decomposition temperature and the time required for complete decomposition was determined. On the basis of the information from STA, the thermolysis procedure described in the preceding section was chosen.

The morphology of the tapes was investigated by scanning electron microscopy (SEM; Tescan 5130MM, Czech Republic) under 20 kV accelerating voltage. For cross sectional images, tapes were secured to 45° sample holders using carbon adhesive tabs.

The molar carbon to oxygen ratio (C/O) of the samples, which provides an overview of the changes in FGSs during heat treatments, was determined by CHO (combustion) chemical analysis (Atlantic Microlab Inc., Norcross, GA).

To analyze FGS spacing and the degree of graphitization in tape samples, X-ray diffraction (XRD) patterns were obtained using a desktop diffractometer (Rigaku MiniFlex II, Cu K_α radiation at λ = 1.54 Å, The Woodlands, TX) sampling at 2° min^{-1}, 30 kV and 15 mA.

Surface area was determined from the nitrogen adsorption by the Brunauer, Emmett, and Teller (BET) method[46] using a surface area analyzer (Gemini V, Micromeritics Instrument Corporation, Norcross, GA). Eleven data points were taken for each fit from a relative pressure of 0.05−0.30, with an equilibrium time of 5 s, an evacuation rate of 13.3 $kPa \cdot min^{-1}$ (100 $mmHg \cdot min^{-1}$), and an evacuation time of 2 min. Samples were dried for 3 h at 200 °C under vacuum before measurement.

Electrical conductivity measurements were made similarly to the described ISO3915 standard procedure.[47] Copper tapes (3M, St. Paul, MN) were attached to the two sides of a rectangular piece of graphene tape or compressed pellet and a constant current of 2−10 mA was applied using a potentiostat (SP-150, BioLogic, Knoxville, TN). For compressed pellets, carbon paste (Electron Microscopy Sciences, Hatfield, PA) was applied between the sample and the copper tape in order to ensure equipotential cross sectional areas. The potential difference between two points along the direction of the current flow was simultaneously recorded for 20 s using the same potentiostat. The average potential drop and the applied current were used to calculate the conductivity of the samples using the formula

$$\sigma = \frac{I}{V} \cdot \frac{\ell}{A}$$

where I, V, ℓ, and A are the applied current, measured potential difference, distance between the two points where the potential difference is measured, and the cross sectional area for the current flow, respectively.

Mechanical testing was done using a load frame (Instron model 5567A, Instron, Norwood, MA) equipped with pneumatic grips with rubber faces. Dogbone-shaped samples were cut from composite tapes using a punch of the appropriate shape and size. Samples were 4.55 mm wide and 22.55 mm long. Following thermolysis, the reduced and the annealed samples were tested under tensile load applied at a velocity of 1 $mm \cdot min^{-1}$.

Acknowledgment. This work was supported by the Army Research Office Multidisciplinary University Research Institute (ARO/MURI) under Grant No. W911NF-09-1-0476 and the Pacific Northwest National Laboratory under Grant No. DE-AC05-76RL01830. J. D. Roy-Mayhew received stipend support through the National Science Foundation Graduate Research Fellowship under Grant No. DGE-0646086. We thank J. Liu, Pacific Northwest National Laboratory (Richland, WA) for TEM of FGS materials.

Supporting Information Available: Further information on the properties of the tape casting suspensions and FGS tapes. This material is available free of charge *via* the Internet at http://pubs.acs.org.

REFERENCES AND NOTES

1. Wang, D.; Choi, D.; Li, J.; Yang, Z.; Nie, Z.; Kou, R.; Hu, D.; Wang, C.; Saraf, L. V.; Zhang, J.; *et al.* Self-Assembled TiO_2 Graphene Hybrid Nanostructures for Enhanced Li-Ion Insertion. *ACS Nano* **2009**, *3*, 907–914.
2. Wang, D.; Kou, R.; Choi, D.; Yang, Z.; Nie, Z.; Li, J.; Saraf, L. V.; Hu, D.; Zhang, J.; Graff, G. L.; *et al.* Ternary Self-Assembly of Ordered Metal Oxide−Graphene Nanocomposites for Electrochemical Energy Storage. *ACS Nano* **2010**, *4*, 1587–1595.
3. Shao, Y.; Wang, J.; Wu, H.; Liu, J.; Aksay, I. A.; Lin, Y. Graphene Based Electrochemical Sensors and Biosensors: A Review. *Electroanal.* **2010**, *22*, 1027–1036.
4. Roy-Mayhew, J. D.; Bozym, D. J.; Punckt, C.; Aksay, I. A. Functionalized Graphene as a Catalytic Counter Electrode in Dye-Sensitized Solar Cells. *ACS Nano* **2010**, *4*, 6203–6211.
5. Hu, Y. H.; Wang, H.; Hu, B. Thinnest Two-Dimensional Nanomaterial—Graphene for Solar Energy. *ChemSusChem* **2010**, *3*, 782–796.
6. Stoller, M. D.; Park, S.; Zhu, Y.; An, J.; Ruoff, R. S. Graphene-Based Ultracapacitors. *Nano Lett.* **2008**, *8*, 3498–3502.
7. Li, X.; Zhang, G.; Bai, X.; Sun, X.; Wang, X.; Wang, E.; Dai, H. Highly Conducting Graphene Sheets and Langmuir−Blodgett Films. *Nat. Nanotechnol.* **2008**, *3*, 538–542.
8. Haiqun, C.; Marc, B. M.; Kerry, J. G.; Gordon, G. W.; Dan, L. Mechanically Strong, Electrically Conductive, and Biocompatible Graphene Paper. *Adv. Mater.* **2008**, *20*, 3557–3561.
9. Dikin, D. A.; Stankovich, S.; Zimney, E. J.; Piner, R. D.; Dommett, G. H. B.; Evmenenko, G.; Nguyen, S. T.; Ruoff, R. S. Preparation and Characterization of Graphene Oxide Paper. *Nature* **2007**, *448*, 457–460.
10. Mistler, R. E.; Twiname, E. R. *Tape Casting. Theory and Practice*; American Ceramic Society: Westerville, OH, 2000.
11. Schniepp, H. C.; Li, J.-L.; McAllister, M. J.; Sai, H.; Herrera-Alonso, M.; Adamson, D. H.; Prud'homme, R. K.; Car, R.; Saville, D. A.; Aksay, I. A. Functionalized Single Graphene Sheets Derived from Splitting Graphite Oxide. *J. Phys. Chem. B* **2006**, *110*, 8535–8539.
12. McAllister, M. J.; Li, J.-L.; Adamson, D. H.; Schniepp, H. C.; Abdala, A. A.; Liu, J.; Herrera-Alonso, M.; Milius, D. L.; Car, R.; Prud'homme, R. K.; Aksay, I. A. Single Sheet Functionalized Graphene by Oxidation and Thermal Expansion of Graphite. *Chem. Mater.* **2007**, *19*, 4396–4404.
13. Li, J.-L.; Kudin, K. N.; McAllister, M. J.; Prud'homme, R. K.; Aksay, I. A.; Car, R. Oxygen-Driven Unzipping of Graphitic Materials. *Phys. Rev. Lett.* **2006**, *96*, 176101.
14. Punckt, C.; Pope, M. A.; Liu, J.; Lin, Y.; Aksay, I. A. Electrochemical Performance of Graphene as Effected by Electrode Porosity and Graphene Functionalization. *Electroanal.* **2010**, *22*, 2834–2841.

15. Sabourin, J. L.; Dabbs, D. M.; Yetter, R. A.; Dryer, F. L.; Aksay, I. A. Functionalized Graphene Sheet Colloids for Enhanced Fuel/Propellant Combustion. *ACS Nano* **2009**, *3*, 3945–3954.
16. Kou, R.; Shao, Y.; Mei, D.; Nie, Z.; Wang, D.; Wang, C.; Viswanathan, V. V.; Park, S.; Aksay, I. A.; Lin, Y.; *et al*. Stabilization of Electrocatalytic Metal Nanoparticles at Metal−Metal Oxide−Graphene Triple Junction Points. *J. Am. Chem. Soc.* **2011**, *133*, 2541–2547.
17. Napper, D. H.; Netschey, A. Studies of the Steric Stabilization of Colloidal Particles. *J. Colloid Interface Sci.* **1971**, *37*, 528–535.
18. Almog, Y.; Klein, J. Interactions between Mica Surfaces in a Polystyrene—Cyclopentane Solution near the θ Temperature. *J. Colloid Interface Sci.* **1985**, *106*, 33–44.
19. Alexandridis, P.; Hatton, T. A. Poly(ethylene oxide)—Poly(propylene oxide)—Poly(ethylene oxide) Block Copolymer Surfactants in Aqueous Solutions and at Interfaces: Thermodynamics, Structure, Dynamics, and Modeling. *Colloids Surf., A* **1995**, *96*, 1–46.
20. Russel, W. B.; Saville, D. A.; Schowalter, W. R. *Colloidal Dispersions*; Cambridge University Press: Cambridge, 1989.
21. Israelachvili, J. N.; Tirrell, M.; Klein, J.; Almog, Y. A. Forces Between Two Layers of Adsorbed Polystyrene Immersed in Cyclohexane below and above the θ Temperature. *Macromolecules* **1984**, *17*, 204–209.
22. Bihannic, I.; Baravian, C.; Duval, J. F. L.; Paineau, E.; Meneau, F.; Levitz, P.; de Silva, J. P.; Davidson, P.; Michot, L. J. Orientational Order of Colloidal Disk-Shaped Particles under Shear-Flow Conditions: A Rheological−Small-Angle X-ray Scattering Study. *J. Phys. Chem. B* **2010**, *114*, 16347–16355.
23. Ebagninin, K. W.; Benchabane, A.; Bekkour, K. Rheological Characterization of Poly(ethylene oxide) Solutions of Different Molecular Weights. *J. Colloid Interface Sci.* **2009**, *336*, 360–367.
24. Decker, E. L.; Garoff, S. Contact Line Structure and Dynamics on Surfaces with Contact Angle Hysteresis. *Langmuir* **1997**, *13*, 6321–6332.
25. Meng, Q.; Higdona, J. J. L. Large Scale Dynamic Simulation of Plate-Like Particle Suspensions. Part II: Brownian Simulation. *J. Rheol.* **2008**, *52*, 37–65.
26. Van De Ven, T. G. M.; Takamura, K.; Mason, S. G. The Microrheology of Colloidal Dispersions: X. Rotations of Spheroids at High Péclet Numbers. *J. Colloid Interface Sci.* **1981**, *82*, 373–383.
27. Geim, A. K.; Novoselov, K. S. The Rise of Graphene. *Nat. Mater.* **2007**, *6*, 183–191.
28. Si, Y.; Samulski, E. T. Exfoliated Graphene Separated by Platinum Nanoparticles. *Chem. Mater.* **2008**, *20*, 6792–6797.
29. Endo, M.; Kim, C.; Hiraoka, T.; Karaki, T.; Nishimura, K.; Matthews, M. J.; Brown, S. D. M.; Dresselhaus, M. S. Structural Characterization of Carbons Obtained from Polyparaphenylenes Prepared by the Kovacic and Yamamoto Methods. *J. Mater. Res.* **1998**, *13*, 2023–2030.
30. Jung, I.; Dikin, D. A.; Piner, R. D.; Ruoff, R. S. Tunable Electrical Conductivity of Individual Graphene Oxide Sheets Reduced at "Low" Temperatures. *Nano Lett.* **2008**, *8*, 4283–4287.
31. Seldin, E. J. Sress-Strain Properties of Polycrystalline Graphites in Tension and Compression at Room Temperature. *Carbon* **1966**, *4*, 177–191.
32. Wagner, P.; O'Rourke, J. A.; Armstrong, P. E. Porosity Effects in Polycrystalline Graphite. *J. Am. Ceram. Soc.* **1972**, *55*, 214–219.
33. Gibson, L. J.; Ashby, M. F. The Mechanics of Three-Dimensional Cellular Materials. *Proc. R. Soc. A, Math. Phys.* **1982**, *382*, 43–59.
34. Pekala, R. W.; Alviso, C. T.; LeMay, J. D. Organic Aerogels: Microstructural Dependence of Mechanical Properties in Compression. *J. Non-Cryst. Solids* **1990**, *125*, 67–75.
35. Fan, H.; Hartshorn, C.; Buchheit, T.; Tallant, D.; Assink, R.; Simpson, R.; Kissel, D. J.; Lacks, D. J.; Torquato, S.; Brinker, C. J. Modulus-Density Scaling Behaviour and Framework Architecture of Nanoporous Self-Assembled Silicas. *Nat. Mater.* **2007**, *6*, 418–423.
36. Lee, C.; Wei, X.; Kysar, J. W.; Hone, J. Measurement of the Elastic Properties and Intrinsic Strength of Monolayer Graphene. *Science* **2008**, *321*, 385–388.
37. Jones, W. K.; Liu, Y.; Larsen, B.; Wang, P.; Zampino, M. Chemical, Structural, and Mechanical Properties of the LTCC Tapes. *Int. J. Microcircuits Electron. Packag.* **2000**, *23*, 469–473.
38. McAndrew, T. P. Poly(Propylene Carbonate)-Containing Ceramic Tape Formulations and the Green Tapes Resulting Therefrom. U.S. Patent 5,089,070, February 18, 1992.
39. Anderson, L. C.; Nufer, R. W.; Pugliese, F. G. Ceramic Dielectrics. U.S. Patent 4,387,131, June 7, 1983.
40. Whitten, P. G.; Gestos, A. A.; Spinks, G. M.; Gilmore, K. J.; Wallace, G. G. Free Standing Carbon Nanotube Composite Bio-Electrodes. *J. Biomed. Mater. Res.* **2007**, *82B*, 37–43.
41. Vigolo, B.; Penicaud, A.; Coulon, C.; Sauder, C. d.; Pailler, R.; Journet, C.; Bernier, P.; Poulin, P. Macroscopic Fibers and Ribbons of Oriented Carbon Nanotubes. *Science* **2000**, *290*, 1331–1334.
42. Worsley, M. A.; Kucheyev, S. O.; Satcher, J. J. H.; Hamza, A. V.; Baumann, T. F. Mechanically Robust and Electrically Conductive Carbon Nanotube Foams. *Appl. Phys. Lett.* **2009**, *94*, 073115–3.
43. Worsley, M. A.; Satcher, J. H.; Baumann, T. F. Synthesis and Characterization of Monolithic Carbon Aerogel Nanocomposites Containing Double-Walled Carbon Nanotubes. *Langmuir* **2008**, *24*, 9763–9766.
44. Edie, D. D. The Effect of Processing on the Structure and Properties of Carbon Fibers. *Carbon* **1998**, *36*, 345–362.
45. Guigon, M.; Oberlin, A.; Desarmot, G. Microtexture and Structure of Some High-Modulus, PAN-Based Carbon Fibres. *Fibre Sci. Technol.* **1984**, *20*, 177–198.
46. Brunauer, S.; Emmett, P. H.; Teller, E. Adsorption of Gases in Multimolecular Layers. *J. Am. Chem. Soc.* **1938**, *60*, 309–319.
47. *ISO3915, Measurement of Resistivity of Conductive Plastics*; International Organization for Standardization: Geneva, Switzerland, 1981.
48. Uher, C.; Sander, L. M. Unusual Temperature Dependence of the Resistivity of Exfoliated Graphites. *Phys. Rev. B* **1983**, *27*, 1326.
49. Birgeneau, R. J.; Heiney, P. A.; Pelz, J. P. High Resolution X-ray Studies of Monolayer Krypton on Varied Forms of Graphite. *Phys. B, C* **1982**, *109−110*, 1785–1795.
50. Niimi, Y.; Murakawa, S.; Matsumoto, Y.; Kambara, H.; Fukuyama, H. Characterization of ZYX Exfoliated Graphite for Studies of Monolayer He below 1 mK. *Rev. Sci. Instrum.* **2003**, *74*, 4448–4452.
51. Revilock, J. F. "Grafoil" Graphite Tape—Its Manufacture, Properties and Uses. *Am. Chem. Soc. Div. Fuel Chem.* 1968, *Preprints 12*, 94.
52. Chen, J.-H.; Jang, C.; Xiao, S.; Ishigami, M.; Fuhrer, M. S. Intrinsic and Extrinsic Performance Limits of Graphene Devices on SiO_2. *Nat. Nanotechnol.* **2008**, *3*, 206–209.
53. De, S.; Coleman, J. N. Are There Fundamental Limitations on the Sheet Resistance and Transmittance of Thin Graphene Films? *ACS Nano* **2010**, *4*, 2713–2720.
54. Spain, I. L.; Ubbelohde, A. R.; Young, D. A. Electronic Properties of Well-Oriented Graphite. *Philos. Trans. R. Soc. A* **1967**, *262*, 345–386.
55. Pierson, H. O. *Handbook of Carbon, Graphite, Diamond, and Fullerenes*; Noyes Publications; Park Ridge, NJ, 1993.
56. Dowell, M. B.; Howard, R. A. Tensile and Compressive Properties of Flexible Graphite Foils. *Carbon* **1986**, *24*, 311–323.